nature genetics

Supplementary information

https://doi.org/10.1038/s41588-024-01782-y

Body mass index stratification optimizes polygenic prediction of type 2 diabetes in cross-biobank analyses

In the format provided by the authors and unedited

Supplementary Note

Comparing BMI stratification and BMI covariates

We explored how the BMI-stratified or BMI-unstratified PRSs predictions would change when BMI is included in the model as covariates to clarify the discrepancy between BMI stratification and BMI adjustment. We observed that the liability R^2 for the low BMI targets was significantly improved in all conditions regardless of BMI adjustment ($P < 1.0 \times 10^{-4}$ for all; **Extended Data Fig. 4** and **Supplementary Table 5**). We replicated similar results within the full model AUC evaluation as with R^2 (**Extended Data Fig. 5**). The results of full model AUC also showed that BMI stratification provides greater improvements in absolute values of AUC compared to BMI adjustment as covariates. These results are consistent with the previous studies that showed only minimal differences in effect sizes for most T2D-associated variants in comparisons with and without BMI adjustment as covariates[38,39].

Pathway clustering without variant filtering

Udler's clustering applies weight filtering to each variant and assigns the variant to the highest-weighted pathway. Thus, strictly written, Udler's clustering is soft clustering at the individual level, but exclusive clustering method at the variant level. Then, we also confirmed the results of soft clustering without variant filtering (**Supplementary Figs. 8–11**). Since the assigned variants in each pathway cluster increased, all clusters showed nominally significant improvement of polygenic prediction in the low BMI groups (**Supplementary Table 9**). We note that the unfiltered method does not keep independence among clusters since each pathway cluster partially shares the variants and corresponding genes.

Assessment by net reclassification improvement

To quantitatively assess the clinical impact of PRSs for individual risk under BMI stratification, we calculated net reclassification improvement (NRI) from the model without PRSs to the model including PRSs[45–47]. For calculating the categorical NRI, we adopted the percentile-based NRI with the threshold based on the case-control ratio of the dataset[48]. We also calculated the continuous NRI, which is an objective and comparable index without the bias of setting a threshold[49]. The results in BBJ showed that low BMI group showed significantly higher categorical NRI than that of high BMI group ($P = 1.4 \times 10^{-4}$,

0.154 for low BMI and 0.123 for high BMI; **Supplementary Fig. 14,** and **Supplementary Table 11**). Continuous NRI showed similar results in BBJ ($P = 6.2 \times 10^{-5}$, 0.277 for low BMI and 0.221 for high BMI; **Supplementary Table 11**). In UKBB, the low BMI group showed significantly higher categorical NRI than that of high BMI group ($P = 0.017$, 0.099 for low BMI and 0.081 for high BMI, **Supplementary Fig. 15,** and **Supplementary Table 12**). Continuous NRI also showed concordant results to UKBB ($P = 2.4 \times 10^{-4}$, 0.245 for low BMI and 0.193 for high BMI; **Supplementary Table 12**). We also confirmed that the results could be replicated in independent cohorts, Tohoku Medical Megabank Project (TMM) and the second cohort of BBJ (BBJ-2nd). NRIs in TMM showed the concordant direction while not significant (**Supplementary Fig. 18,** and **Supplementary Table 13**), and BBJ-2nd showed significantly higher NRIs in the low BMI group than in the high BMI group ($P = 1.8 \times 10^{-4}$ in categorical NRI, $P = 2.4 \times 10^{-5}$ in continuous NRI, **Supplementary Fig. 19,** and **Supplementary Table 14**).

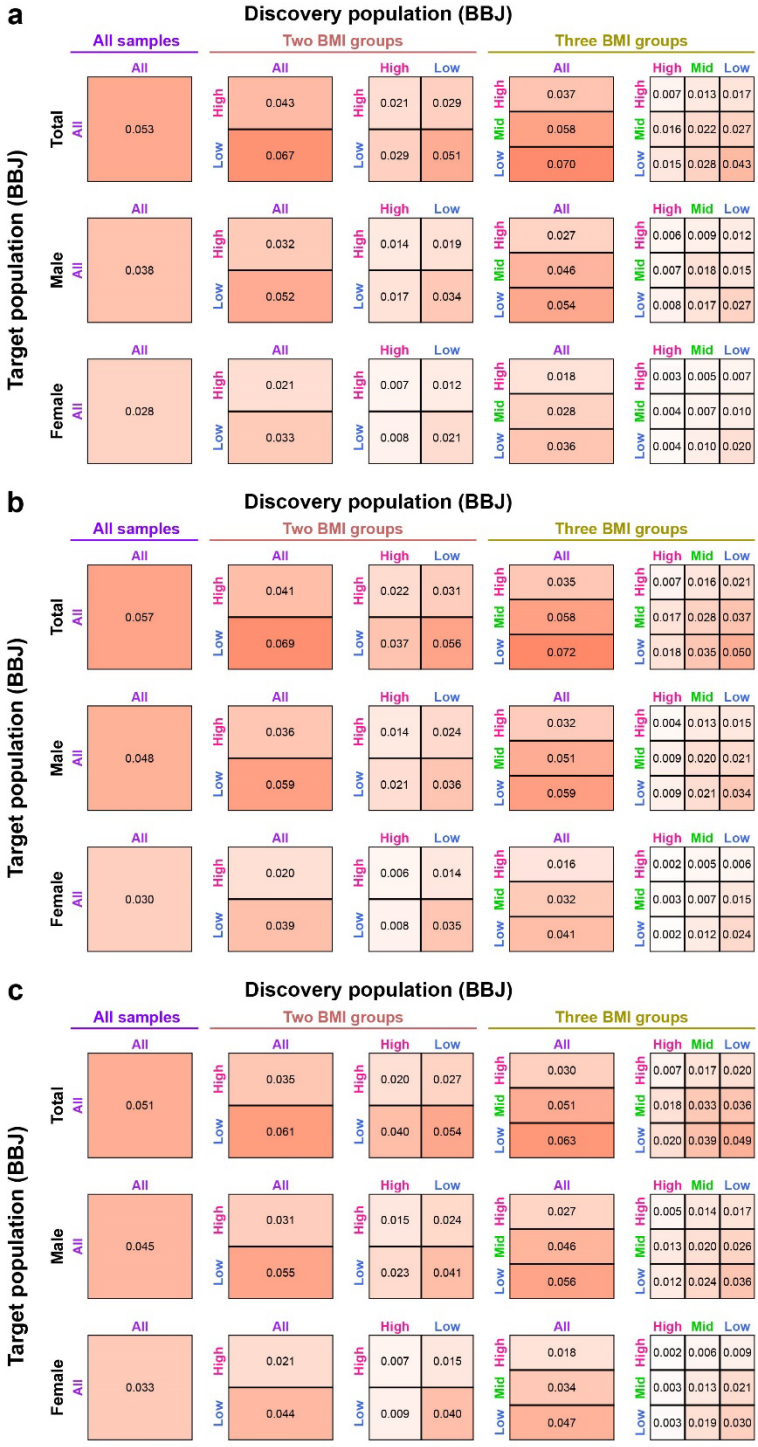

Supplementary Fig. 1 | BMI-stratified PRS heatmaps for T2D in BBJ (C+T). PRS heatmaps were performed with the clumping and thresholding method instead of the Bayesian method. We show a PRS heatmaps of three *P*-thresholds. The *P*-thresholds from top to bottom are: 1e-2 (**a**), 1e-3 (**b**), 1e-4 (**c**).

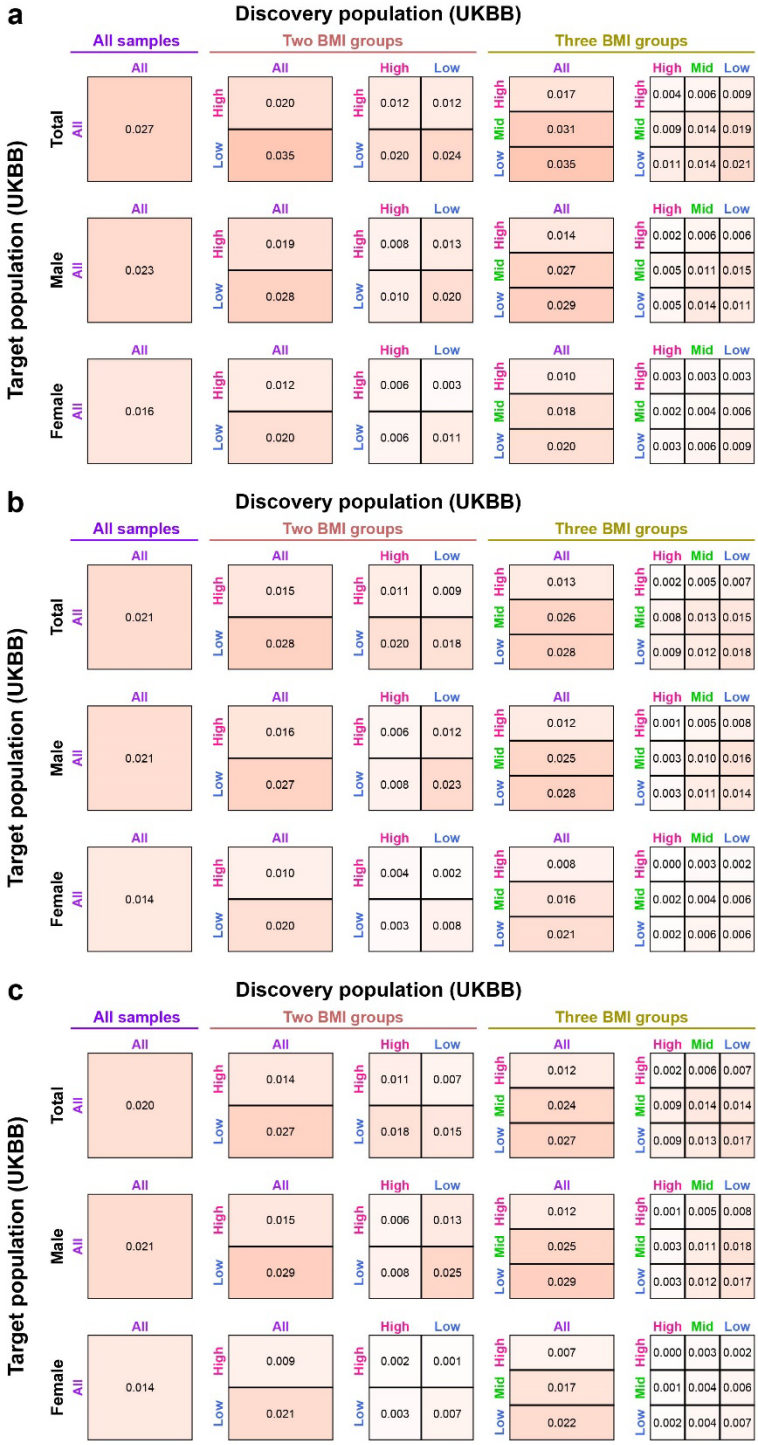

Supplementary Fig. 2 | BMI-stratified PRS heatmaps for T2D in UKBB (C+T). PRS heatmaps were performed with the clumping and thresholding method instead of the Bayesian method. We show a PRS heatmaps of three *P*-thresholds. The *P*-thresholds from top to bottom are: 1e-2 (**a**), 1e-3 (**b**), 1e-4 (**c**).

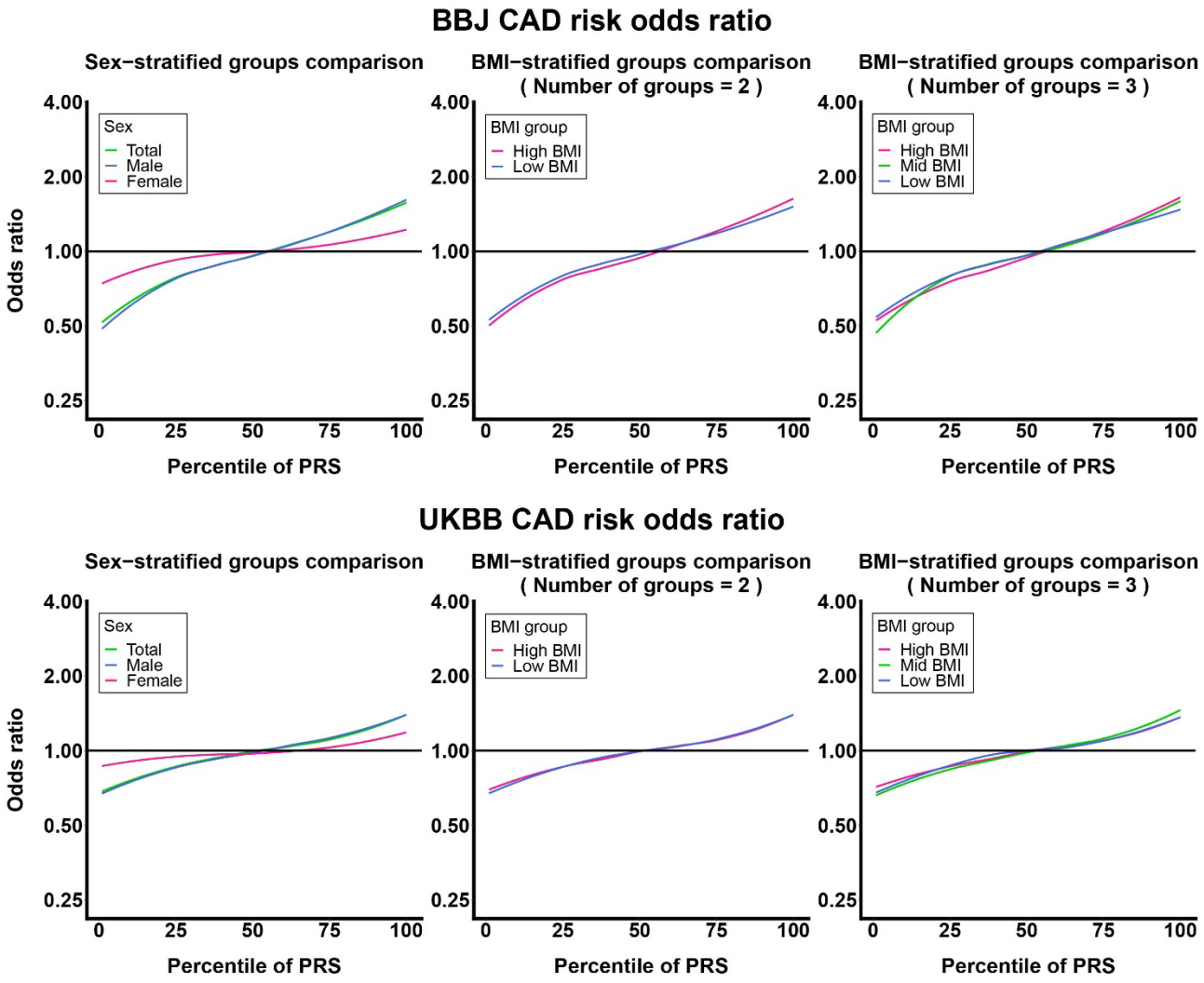

Supplementary Fig. 3 | Odds ratio curve of CAD prevalence for each BMI-stratified PRS. Odds ratio curves for each BMI-stratified PRS in each box are locally estimated scatterplot smoothing (LOESS) curves. On the left, a comparison is made between male and female samples and the total samples; in the middle, two BMI-stratified groups of the total samples; on the right, three BMI-stratified groups of the total samples. **a** Odds ratio curves for T2D in BBJ. **b** Odds ratio curves for T2D in UKBB.

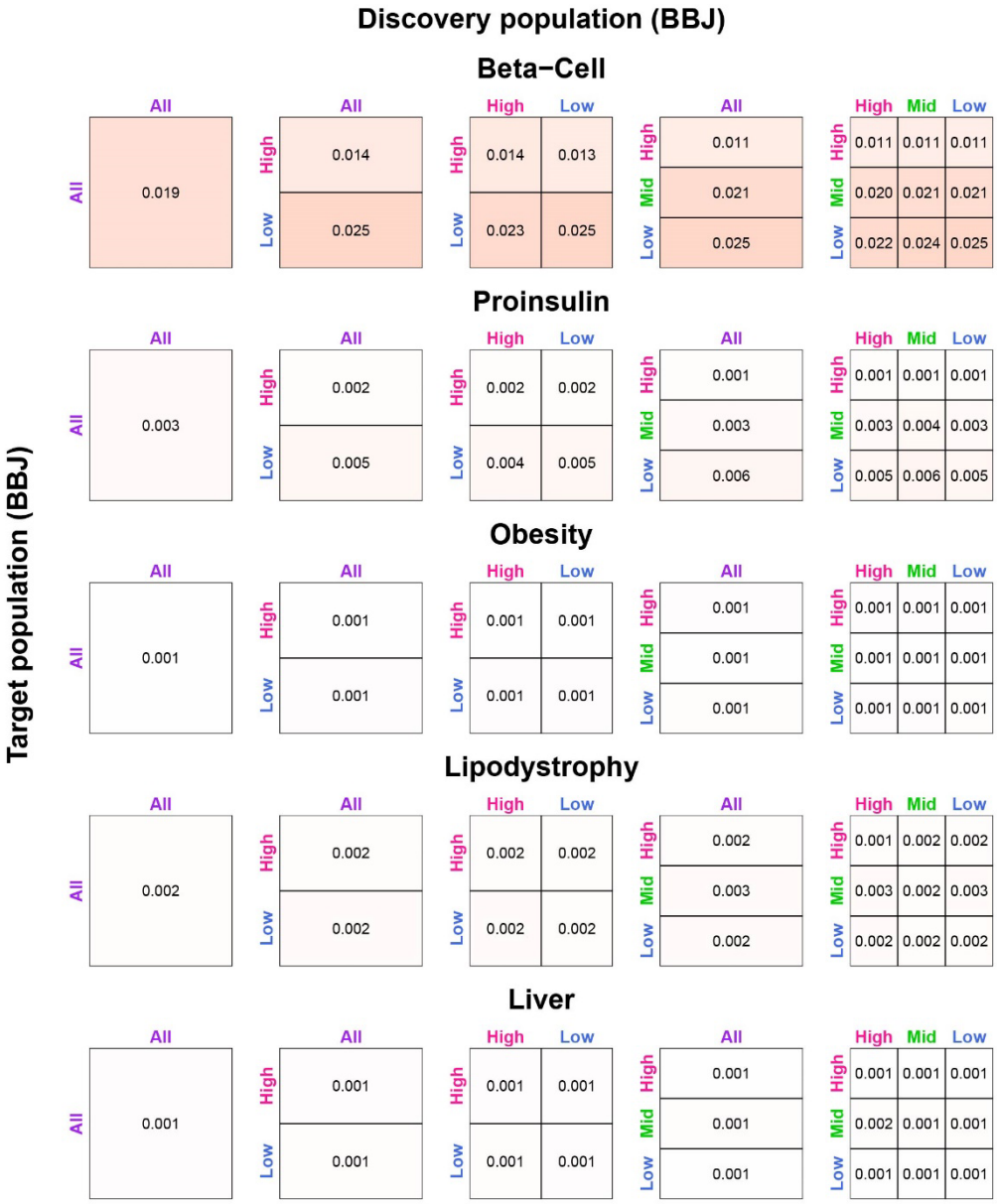

Supplementary Fig. 4 | BMI-stratified PRS heatmaps of T2D in BBJ for each pathogenic pathway. PRS heatmaps with different pathogenic pathways of a soft clustering model can be compared vertically. The values in PRS heatmaps are Fisher's z-transformation averages of pseudo-R^2 calculated by the LOGO-PRS method. Red, high polygenic prediction accuracy; white, low polygenic prediction accuracy. The upper description of the heatmap represents the BMI group of the discovery population, and the left side represents that of the target population.

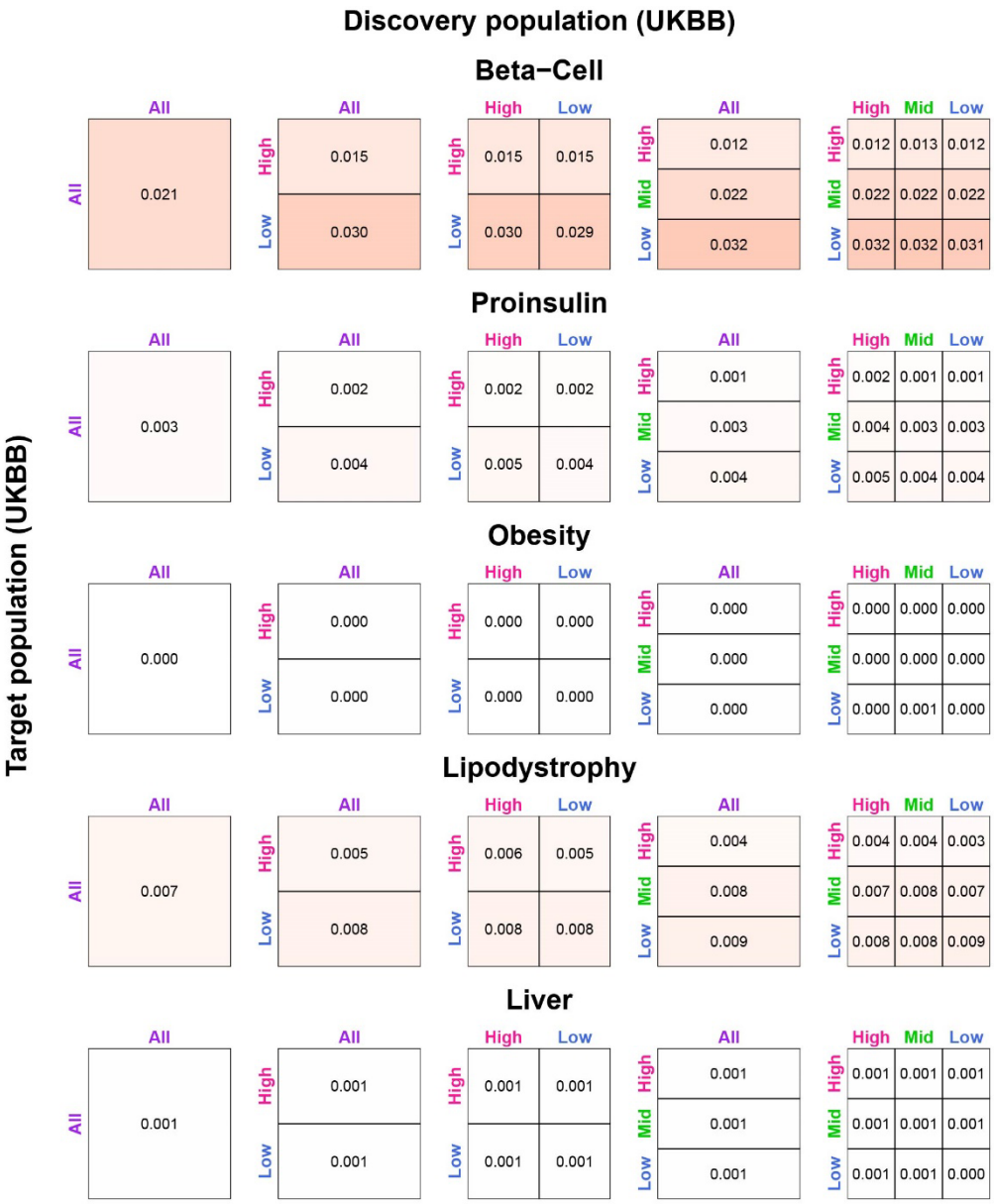

Supplementary Fig. 5 | BMI-stratified PRS heatmaps of T2D in UKBB for each pathogenic pathway. PRS heatmaps with different pathogenic pathways of a soft clustering model can be compared vertically. The values in PRS heatmaps are Fisher's z-transformation averages of pseudo-R^2 calculated by the LOGO-PRS method. Red, high polygenic prediction accuracy; white, low polygenic prediction accuracy. The upper description of the heatmap represents the BMI group of the discovery population, and the left side represents that of the target population.

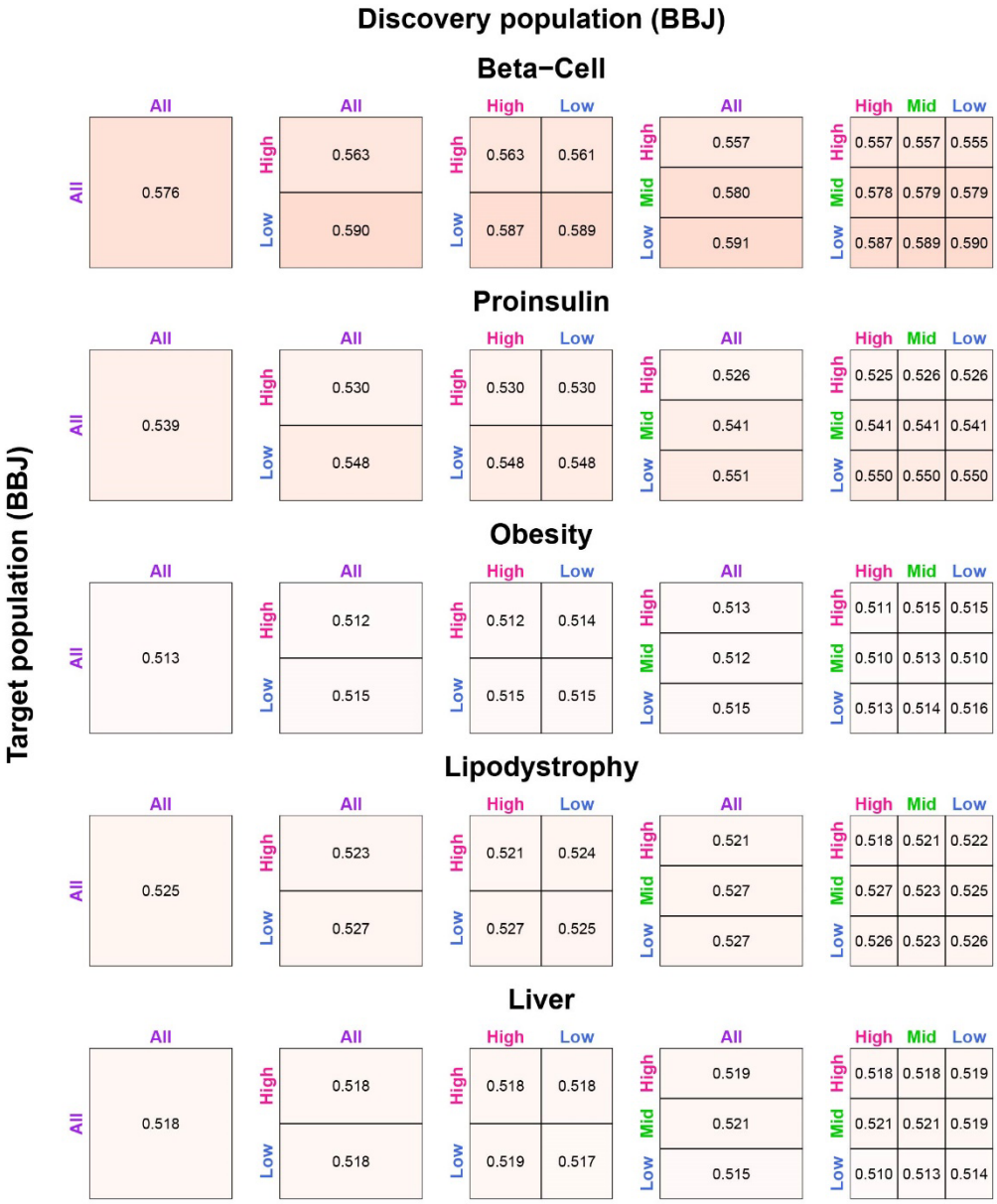

Supplementary Fig. 6 | BMI-stratified PRS heatmaps of T2D in BBJ for each pathogenic pathway evaluated using AUC. PRS heatmaps with different pathogenic pathways of a soft clustering model can be compared vertically. The values in PRS heatmaps are calculated by simple model AUC. Red, high polygenic prediction accuracy; white, low polygenic prediction accuracy. The upper description of the heatmap represents the BMI group of the discovery population, and the left side represents that of the target population.

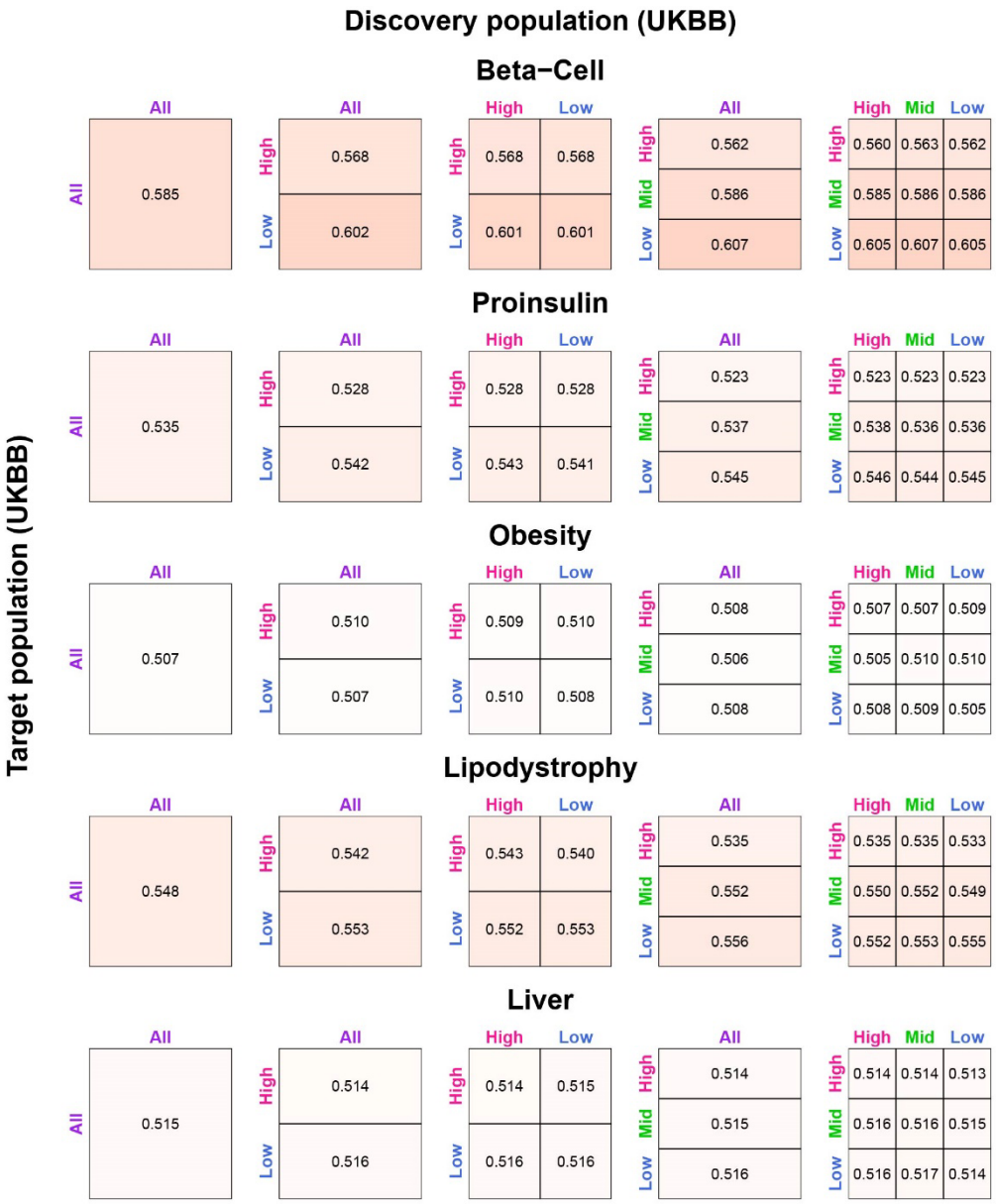

Supplementary Fig. 7 | BMI-stratified PRS heatmaps of T2D in UKBB for each pathogenic pathway evaluated using AUC. PRS heatmaps with different pathogenic pathways of a soft clustering model can be compared vertically. The values in PRS heatmaps are calculated by simple model AUC. Red, high polygenic prediction accuracy; white, low polygenic prediction accuracy. The upper description of the heatmap represents the BMI group of the discovery population, and the left side represents that of the target population.

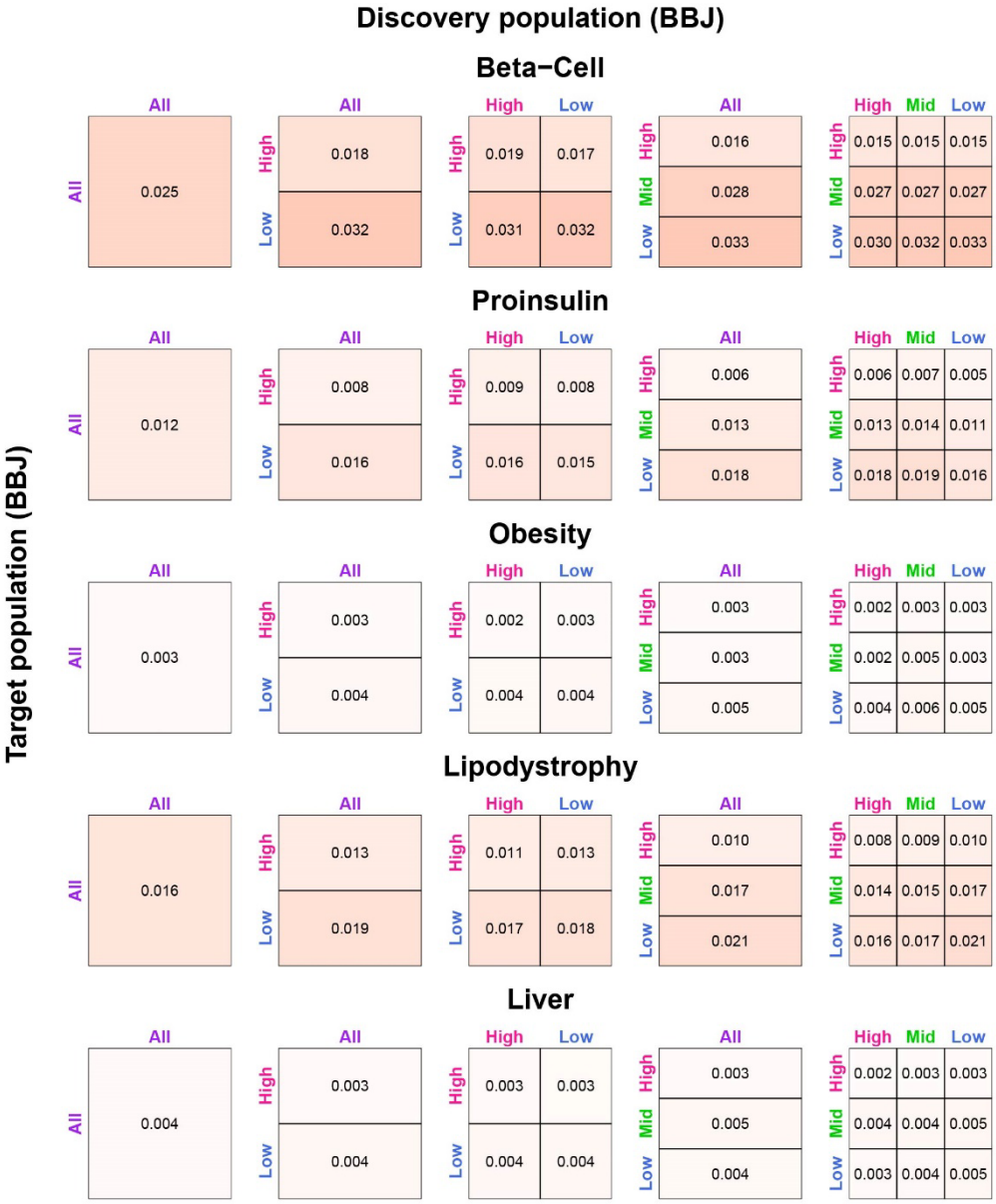

Supplementary Fig. 8 | BMI-stratified PRS heatmaps of T2D in BBJ for each pathogenic pathway without variant filtering. PRS heatmaps with different pathogenic pathways of a soft clustering model can be compared vertically. The values in PRS heatmaps are Fisher's z-transformation averages of pseudo-R^2 calculated by the LOGO-PRS method. Red, high polygenic prediction accuracy; white, low polygenic prediction accuracy. The upper description of the heatmap represents the BMI group of the discovery population, and the left side represents that of the target population.

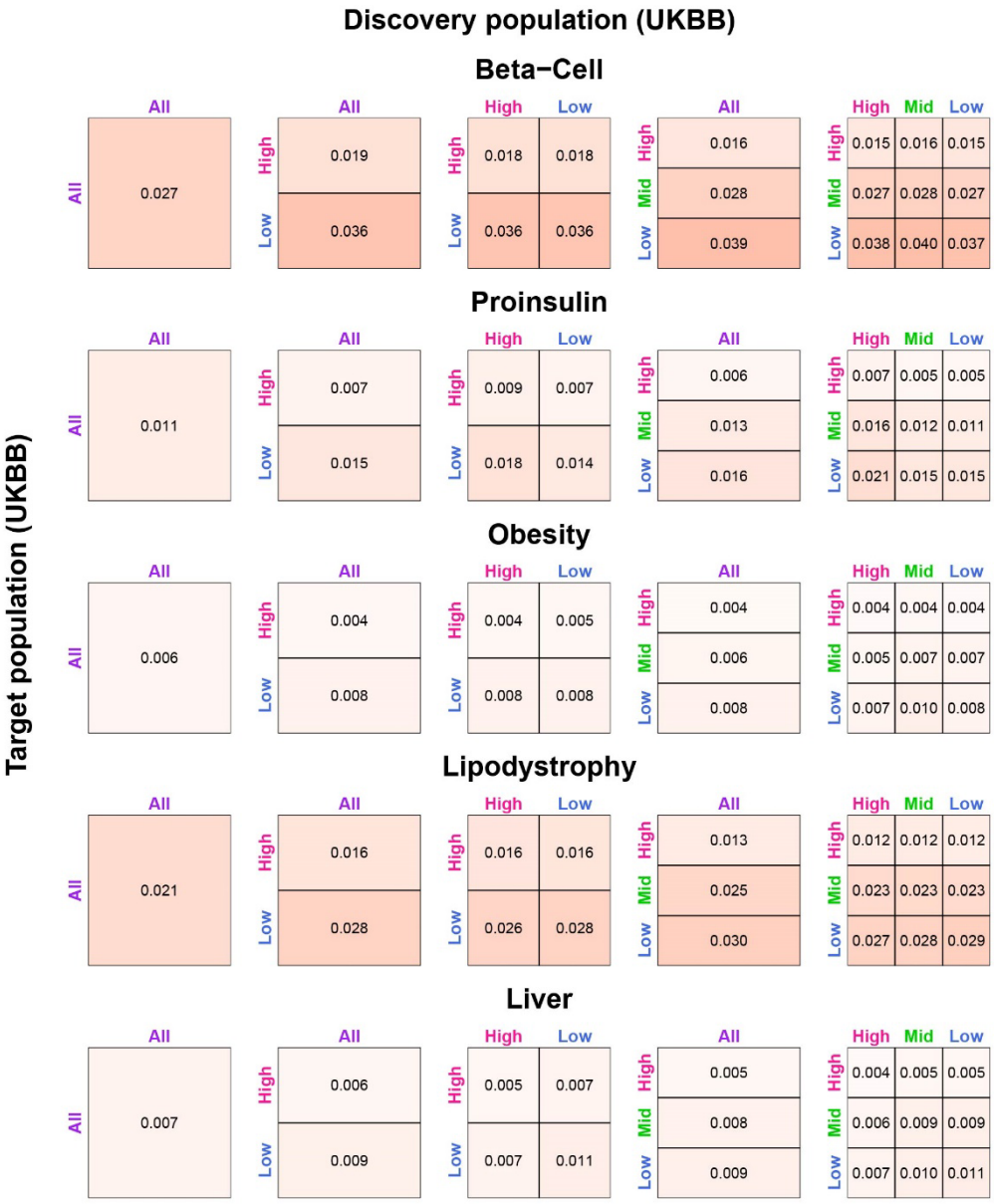

Supplementary Fig. 9 | BMI-stratified PRS heatmaps of T2D in UKBB for each pathogenic pathway without variant filtering. PRS heatmaps with different pathogenic pathways of a soft clustering model can be compared vertically. The values in PRS heatmaps are Fisher's z-transformation averages of pseudo-R^2 calculated by the LOGO-PRS method. Red, high polygenic prediction accuracy; white, low polygenic prediction accuracy. The upper description of the heatmap represents the BMI group of the discovery population, and the left side represents that of the target population.

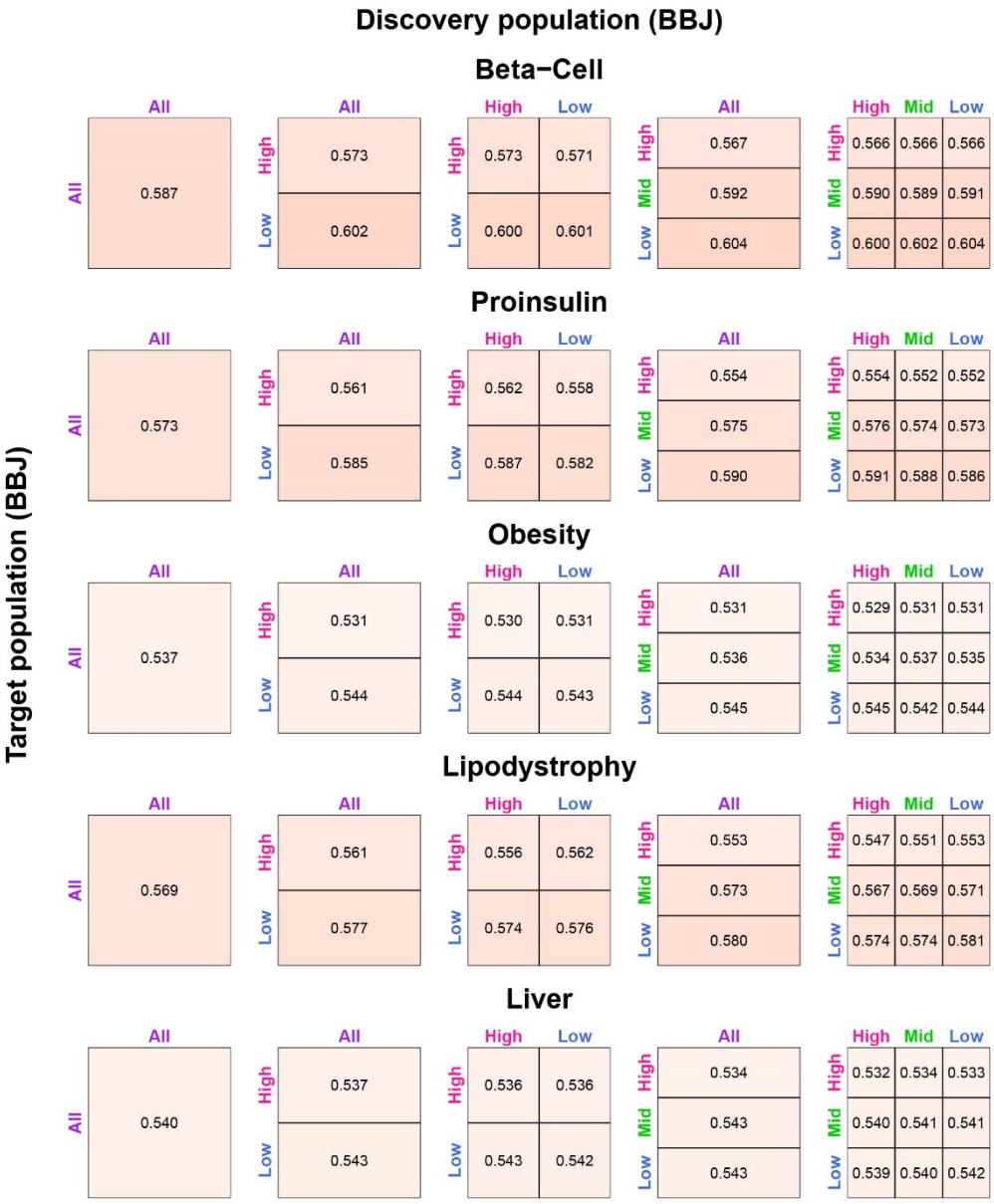

Supplementary Fig. 10 | BMI-stratified PRS heatmaps of T2D in BBJ for each pathogenic pathway without variant filtering evaluated using AUC. PRS heatmaps with different pathogenic pathways of a soft clustering model can be compared vertically. The values in PRS heatmaps are calculated by simple model AUC. Red, high polygenic prediction accuracy; white, low polygenic prediction accuracy. The upper description of the heatmap represents the BMI group of the discovery population, and the left side represents that of the target population.

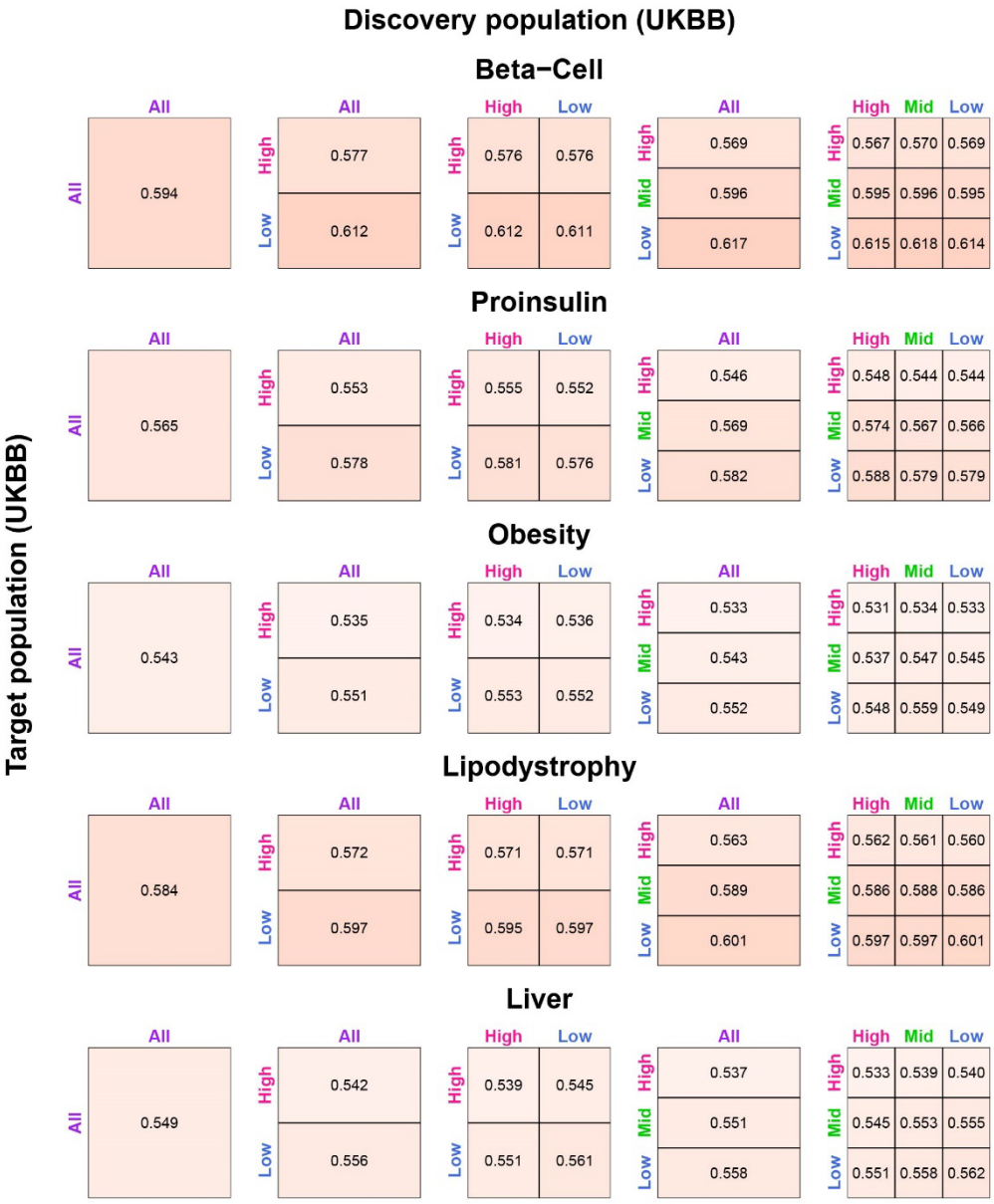

Supplementary Fig. 11 | BMI-stratified PRS heatmaps of T2D in UKBB for each pathogenic pathway without variant filtering evaluated using AUC. PRS heatmaps with different pathogenic pathways of a soft clustering model can be compared vertically. The values in PRS heatmaps are calculated by simple model AUC. Red, high polygenic prediction accuracy; white, low polygenic prediction accuracy. The upper description of the heatmap represents the BMI group of the discovery population, and the left side represents that of the target population.

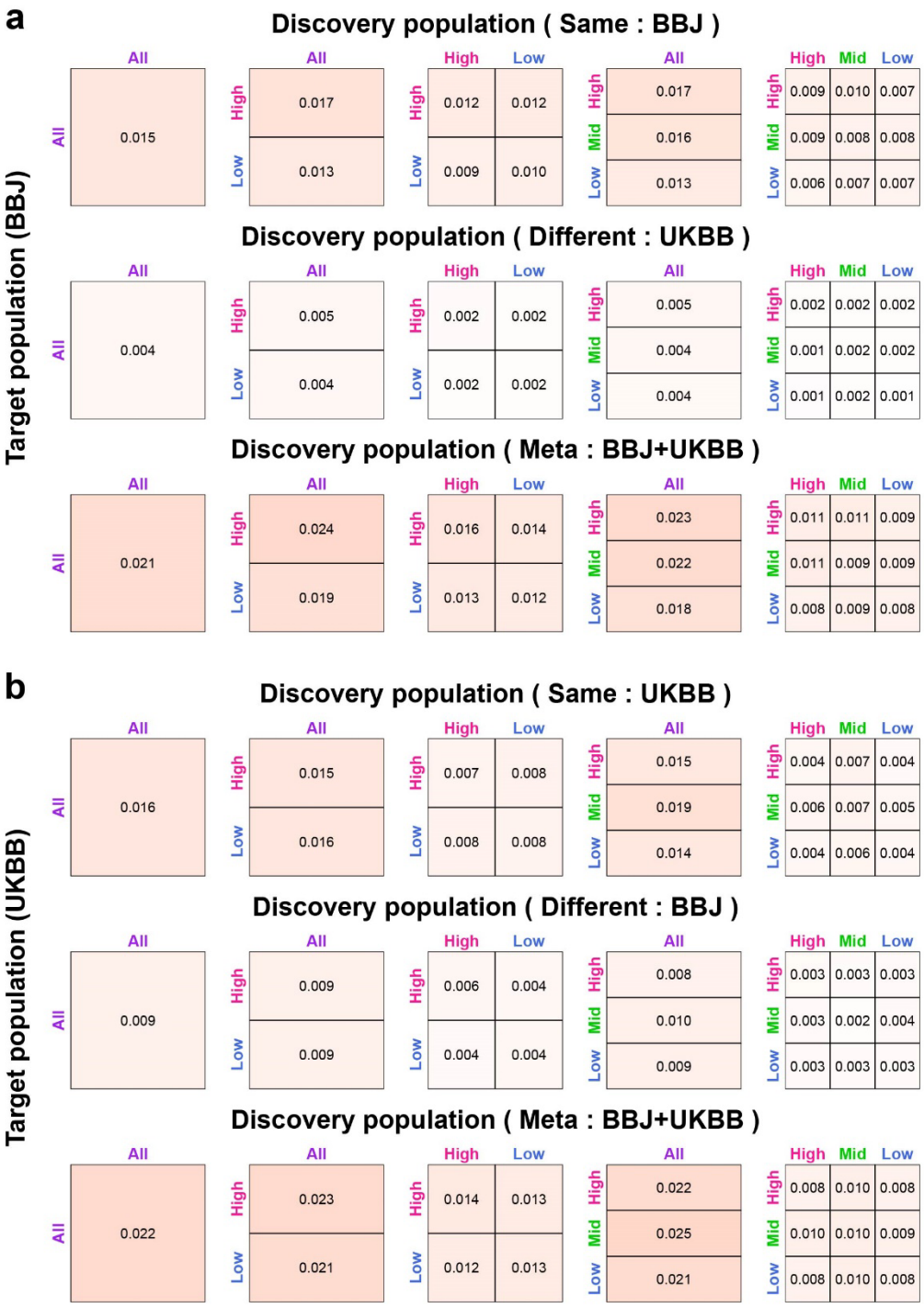

Supplementary Fig. 12 | BMI-stratified PRS heatmaps for CAD across biobanks. PRS heatmaps for the same target with different discovery populations can be compared vertically. The PRS heatmap for the same population coincidences with the total sample in **Figure 4**. **a** PRS heatmaps for CAD with BBJ as target population. **b** PRS heatmaps for CAD with UKBB as target population.

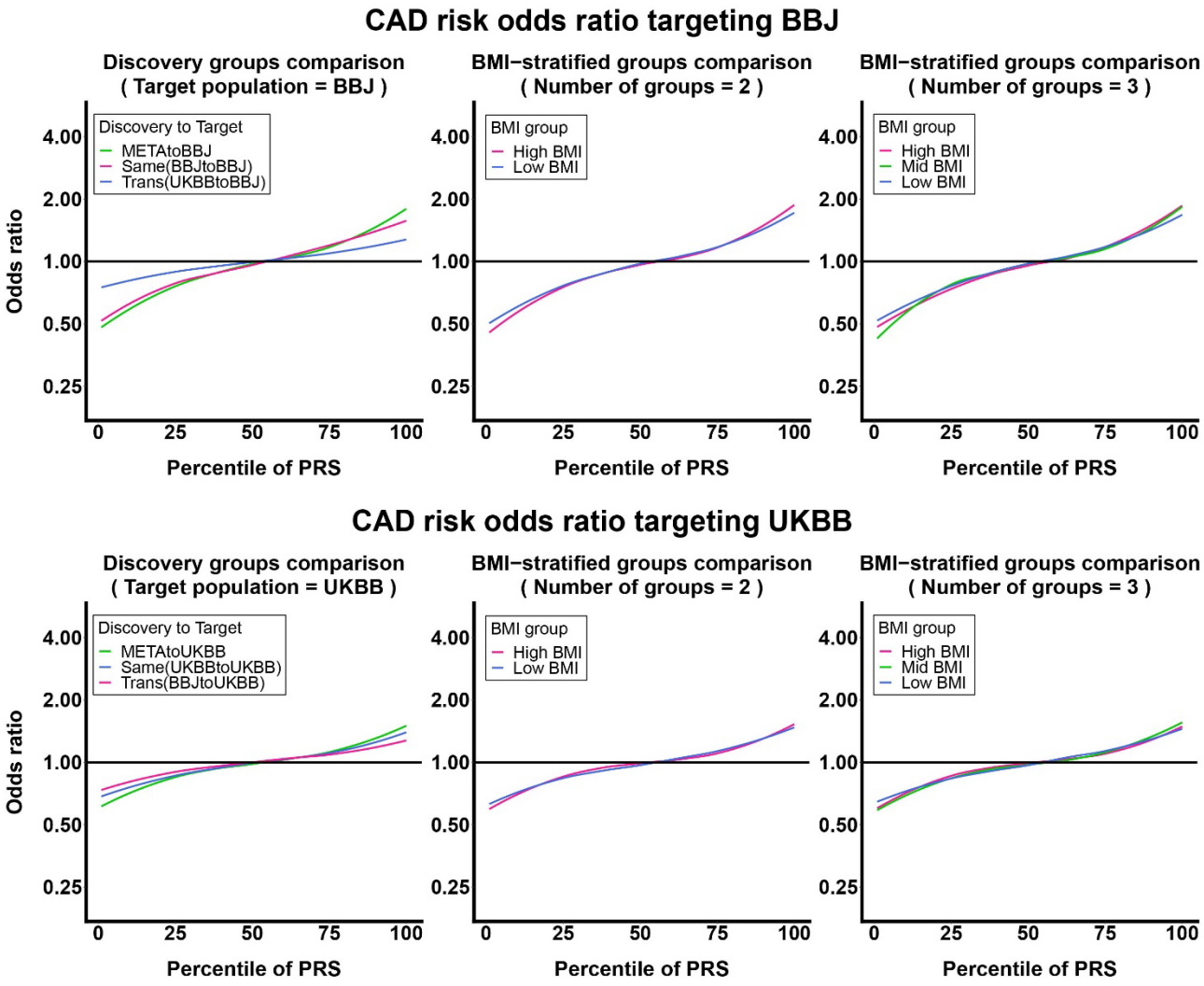

Supplementary Fig. 13 | Odds ratio curve of CAD prevalence for each BMI-stratified PRS across biobanks. Odds ratio curves for each BMI-stratified PRS in each box are locally estimated scatterplot smoothing (LOESS) curves. On the left, the comparison is made with combinations of discovery and target populations; in the middle, two BMI-stratified groups in the meta-populational method; on the right, three BMI-stratified groups in the meta-populational method. **a** Odds ratio curves for CAD with BBJ as target population. **b** Odds ratio curves for CAD with UKBB as target population. High BMI, high BMI group; Mid BMI, middle BMI group; Low BMI, low BMI group; Total, total dataset including both male and female samples.

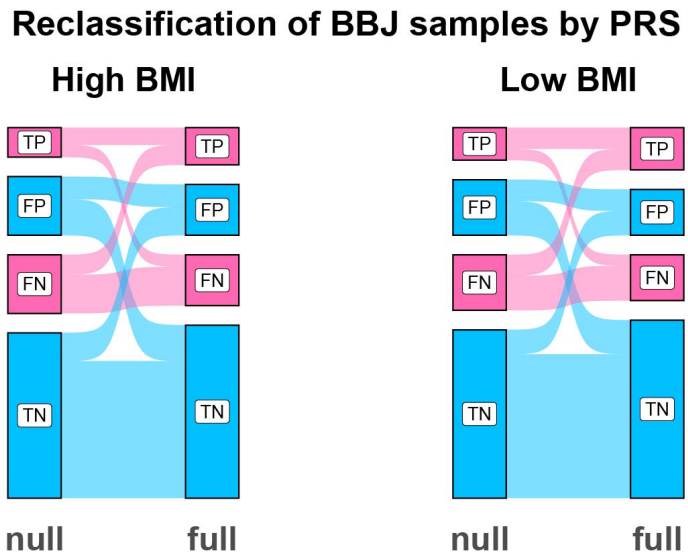

Supplementary Fig. 14 | Sanky diagram of individual reclassification by including PRS in the model for BBJ targets. In each model, individuals with high probability were classified as positive and those with low probability as negative. Pink lines represent case individuals, and light blue lines represent control individuals. TP, true positive; FP, false positive; FN, false negative; TN, true negative.

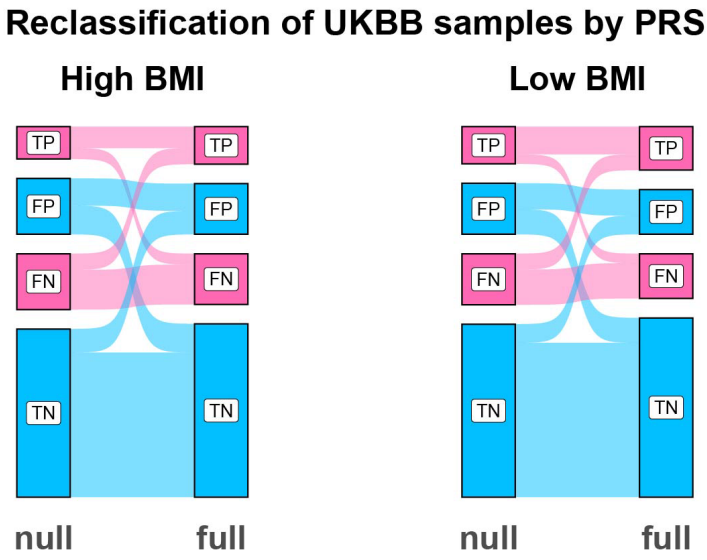

Supplementary Fig. 15 | Sanky diagram of individual reclassification by including PRS in the model for UKBB targets. In each model, individuals with high probability were classified as positive and those with low probability as negative. Pink lines represent case individuals, and light blue lines represent control individuals. TP, true positive; FP, false positive; FN, false negative; TN, true negative.

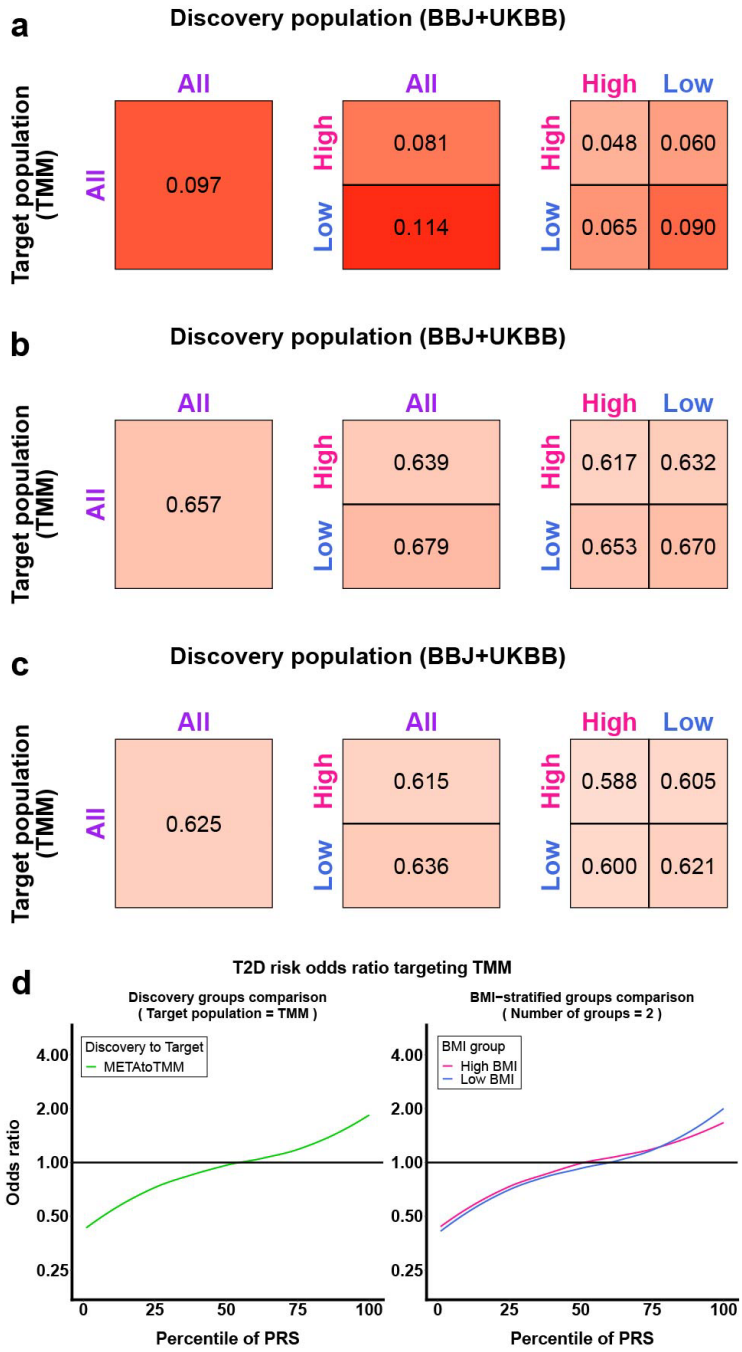

Supplementary Fig. 16 | BMI-stratified PRS heatmaps and Odds ratio curves of T2D in TMM. a PRS heatmaps targeting TMM using PRS calculated from BBJ and UKBB. We defined the cut point for BMI stratification in TMM as BMI = 25, the criterion for obesity in Japan. The values in PRS heatmaps are Fisher's z-transformation averages of pseudo-R^2 calculated by the LOGO-PRS method. **b** The values of PRS heatmaps were calculated by full model AUC. **c** The values of PRS heatmaps were calculated by simple model AUC. **d** Odds ratio curves for each BMI-stratified PRS in each box are locally estimated scatterplot smoothing (LOESS) curves. On the left, odds ratio curve of BMI-unstratified samples; on the right, a comparison is made between two BMI-stratified groups.

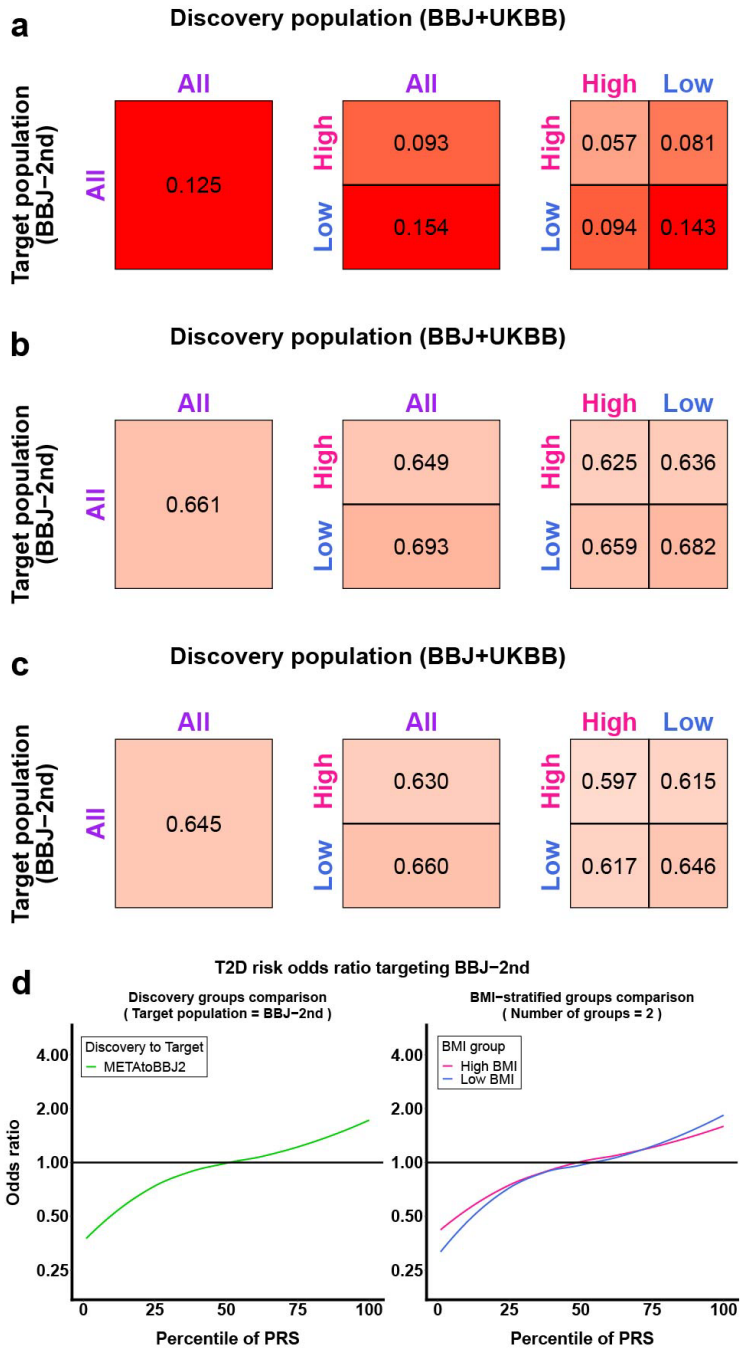

Supplementary Fig. 17 | BMI-stratified PRS heatmaps and Odds ratio curves of T2D in BBJ-2nd. a PRS heatmaps targeting BBJ-2nd using PRS calculated from BBJ and UKBB. We defined the cut point for BMI stratification in BBJ-2nd as BMI = 25, the criterion for obesity in Japan. The values in PRS heatmaps are Fisher's z-transformation averages of pseudo-R^2 calculated by the LOGO-PRS method. **b** The values of PRS heatmaps were calculated by full model AUC. **c** The values of PRS heatmaps were calculated by simple model AUC. **d** Odds ratio curves for each BMI-stratified PRS in each box are locally estimated scatterplot smoothing (LOESS) curves. On the left, odds ratio curve of BMI-unstratified samples; on the right, a comparison is made between two BMI-stratified groups.

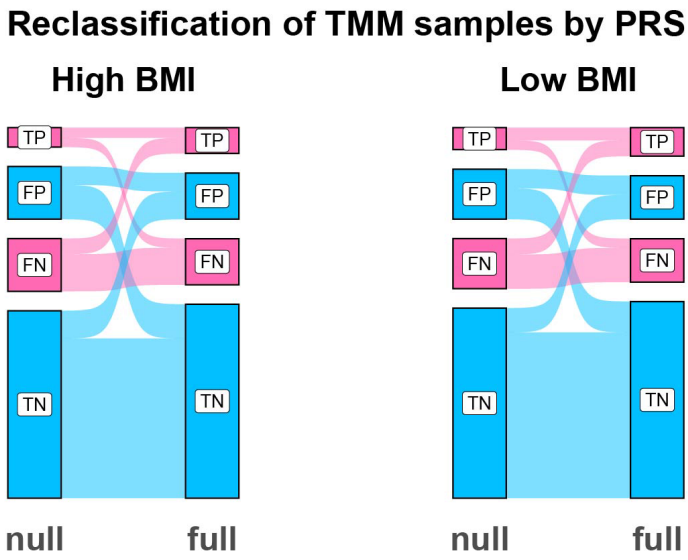

Supplementary Fig. 18 | Sanky diagram of individual reclassification by including PRS in the model for TMM targets. In each model, individuals with high probability were classified as positive and those with low probability as negative. Pink lines represent case individuals, and light blue lines represent control individuals. TP, true positive; FP, false positive; FN, false negative; TN, true negative.

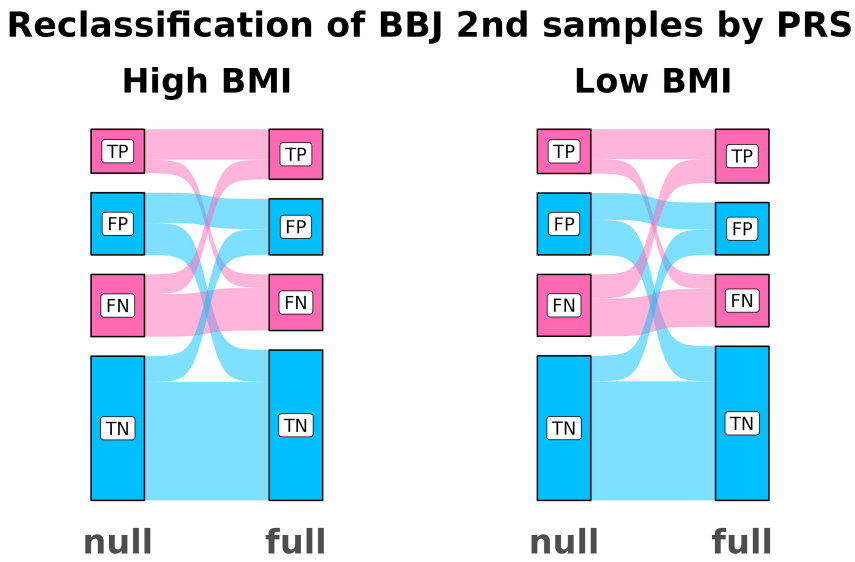

Supplementary Fig. 19 | Sanky diagram of individual reclassification by including PRS in the model for BBJ 2nd cohort targets. In each model, individuals with high probability were classified as positive and those with low probability as negative. Pink lines represent case individuals, and light blue lines represent control individuals. TP, true positive; FP, false positive; FN, false negative; TN, true negative.

BMI cut point	type 2 diabetes				coronary artery disease			
	BBJ		UKBB		BBJ		UKBB	
	Male	Female	Male	Female	Male	Female	Male	Female
1st tertile	24.62	24.03	28.97	28.20	24.98	24.80	30.23	30.48
Median	23.34	22.47	27.30	26.08	23.71	23.28	28.35	28.07
2nd tertile	22.04	21.03	25.80	24.31	22.53	21.85	26.74	26.03

Supplementary Table 1 | BMI values used as cut points for BMI stratification. The median and tertile points of BMI in disease cases were used as cut points for BMI stratification. We set cut points of BMI separately for each of the sex and population groups.

Number of BMI-stratified groups	type 2 diabetes					coronary artery diseases				
	Male Case	Male Control	Female Case	Female Control	Total	Male Case	Male Control	Female Case	Female Control	Total
All samples	17,838	45,330	9,804	24,912	97,884	17,100	56,646	5,550	18,384	97,680
Two BMI groups	8,919	22,665	4,902	12,456	48,942	8,550	28,323	2,775	9,192	48,840
Three BMI groups	5,946	15,110	3,268	8,304	32,628	5,700	18,882	1,850	6,128	32,560

Supplementary Table 2 | Number of total cases and controls in BMI-stratified subsets. The number of samples was adjusted by stratified random sampling based on BMI values to prevent bias in GWAS heritability and polygenic prediction due to differences in the case-control ratios. The samples correspond among three types of stratified data sets. In stratified random sampling, we adjusted the number of case and control samples to match the smallest sample size groups in both biobanks. Thus, we used the same number of samples for the data sets in BBJ and UKBB. Total: the total of all combinations of male/female and case/control.

	T2D		CAD	
	BBJ	**UKBB**	**BBJ**	**UKBB**
Total	1.2×10^{-11}	1.4×10^{-7}	0.0045	0.42
Male	0.0014	7.8×10^{-4}	0.0045	0.14
Female	1.5×10^{-4}	0.15	0.28	0.80

Supplementary Table 3 | *P*-values for likelihood ratio test of BMI-stratified polygenic prediction of T2D. The p-values were calculated by the likelihood ratio test of the group indicator in logistic regression analysis.

	BBJ	UKBB
Total	$<1.0\times10^{-15}$	1.6×10^{-15}
Male	1.1×10^{-5}	1.6×10^{-7}
Female	8.1×10^{-7}	0.020

Supplementary Table 4 | *P*-values for Delong's unpaired test in simple model AUC of BMI-stratified polygenic prediction of T2D. The p-values were calculated by the Delong's unpaired test for simple model AUCs.

	BBJ		UKBB	
	high BMI target	**low BMI target**	**high BMI target**	**low BMI target**
Full AUC	$<1.0\times10^{-15}$	$<1.0\times10^{-15}$	$<1.0\times10^{-15}$	$<1.0\times10^{-15}$
Simple AUC	1.2×10^{-5}	$<1.0\times10^{-15}$	9.4×10^{-5}	1.3×10^{-15}

Supplementary Table 5 | *P*-values for the difference of polygenic prediction of T2D between PRSs generated from high and low BMI discovery GWAS. The p-values were calculated by the Delong's paired test for AUCs.

Discovery	Target	BBJ	UKBB
BMI-unadjusted	**BMI-unadjusted**	1.2×10^{-11}	1.4×10^{-11}
BMI-unadjusted	**BMI-adjusted**	2.0×10^{-10}	8.8×10^{-5}
BMI-adjusted	**BMI-unadjusted**	2.9×10^{-11}	7.7×10^{-9}
BMI-adjusted	**BMI-adjusted**	5.1×10^{-10}	2.1×10^{-5}

Supplementary Table 6 | *P*-values for chi-square test of top 5% samples in BMI-stratified PRS. Covariates related to BMI could be included at two points in the polygenic predictive model, the discovery GWAS and the target regression analysis. We performed polygenic predictions with and without BMI adjustment at these two points and performed a likelihood ratio test of the group indicator in logistic regression analysis.

Complication	High BMI	Low BMI	P (logistic)
Neuropathy	0.205	0.232	4.2×10^{-7}
Retinopathy	0.235	0.281	1.1×10^{-15}
Nephropathy	0.226	0.221	0.39

Supplementary Table 7 | Differences in complication rates between BMI categories in BBJ. Complication rates in the high BMI and low BMI T2D cases in BBJ. The P-value of logistic regression analysis for the difference in complication rates.

Pathway	BBJ		UKBB	
	LRT	Delong	LRT	Delong
BetaCell	5.5×10^{-6}	9.9×10^{-10}	3.0×10^{-10}	1.2×10^{-14}
Proinsulin	0.011	1.8×10^{-4}	0.018	0.017
Obesity	0.58	0.67	0.088	0.10
Lipodystrophy	0.26	0.28	0.15	0.095
Liver	0.94	0.97	0.59	0.68

Supplementary Table 8 | *P*-values of BMI-stratified polygenic prediction of T2D in each pathogenic pathway. LRT, likelihood ratio test of the group indicator in logistic regression analysis; Delong, Delong's unpaired test for simple model AUCs.

Pathway	BBJ		UKBB	
	LRT	Delong	LRT	Delong
BetaCell	3.6×10^{-7}	1.3×10^{-11}	1.8×10^{-11}	1.1×10^{-16}
Proinsulin	3.4×10^{-5}	6.8×10^{-8}	8.0×10^{-7}	2.2×10^{-8}
Obesity	0.26	0.038	0.0011	2.3×10^{-4}
Lipodystrophy	0.030	0.0036	1.7×10^{-5}	4.0×10^{-8}
Liver	0.76	0.58	0.59	0.018

Supplementary Table 9 | *P*-values of BMI-stratified polygenic prediction of T2D in each pathogenic pathway without variant filtering. LRT, likelihood ratio test of the group indicator in logistic regression analysis; Delong, Delong's unpaired test for simple model AUCs.

	BBJ target		UKBB target	
	Meta-PRS	UKBB-PRS	Meta-PRS	BBJ-PRS
Full AUC	5.7×10^{-10}	$<1.0\times10^{-15}$	3.2×10^{-10}	$<1.0\times10^{-15}$
Simple AUC	1.0×10^{-10}	$<1.0\times10^{-15}$	5.5×10^{-13}	$<1.0\times10^{-15}$

Supplementary Table 10 | *P*-values for the difference of polygenic prediction of T2D between PRSs generated from different discovery GWAS. We statistically compared AUCs between same populational model and other populational model, such as meta-populational model or different populational model. The p-values were calculated by the Delong's paired test for AUCs.

	Categorical NRI				Continuous NRI	
	Case	Control	Total	SE	Total	SE
High BMI	0.0880	0.0346	0.1226	0.0058	0.2206	0.0099
Low BMI	0.1103	0.0434	0.1537	0.0057	0.2767	0.0099

Supplementary Table 11 | NRI values of each BMI group in BBJ. For calculating the categorical NRI, we adopted the percentile-based NRI with the threshold based on the case-control ratio of the target dataset. $P = 1.4 \times 10^{-4}$ for categorical NRI and $P = 6.2 \times 10^{-5}$ for continuous NRI. The p-values were calculated by the Z test for NRIs.

	Categorical NRI				Continuous NRI	
	Case	Control	Total	SE	Total	SE
High BMI	0.0585	0.0230	0.0815	0.0053	0.1932	0.0100
Low BMI	0.0711	0.0280	0.0991	0.0051	0.2446	0.0099

Supplementary Table 12 | NRI values of each BMI group in UKBB. For calculating the categorical NRI, we adopted the percentile-based NRI with the threshold based on the case-control ratio of the target dataset. $P = 0.017$ for categorical NRI and $P = 2.4 \times 10^{-4}$ for continuous NRI. The p-values were calculated

by the Z test for NRIs.

	Categorical NRI				Continuous NRI	
	Case	**Control**	**Total**	**SE**	**Total**	**SE**
High BMI	0.0897	0.0269	0.1166	0.0117	0.1915	0.0206
Low BMI	0.0903	0.0271	0.1174	0.0117	0.2185	0.0206

Supplementary Table 13 | NRI values of each BMI group in TMM. For calculating the categorical NRI, we adopted the percentile-based NRI with the threshold based on the case-control ratio of the target dataset. $P = 0.95$ for categorical NRI and $P = 0.35$ for continuous NRI. The p-values were calculated by the Z test for NRIs.

	Categorical NRI				Continuous NRI	
	Case	**Control**	**Total**	**SE**	**Total**	**SE**
High BMI	0.0575	0.0296	0.0870	0.0090	0.1948	0.0163
Low BMI	0.0897	0.0461	0.1358	0.0095	0.2417	0.0162

Supplementary Table 14 | NRI values of each BMI group in BBJ 2nd cohort. For calculating the categorical NRI, we adopted the percentile-based NRI with the threshold based on the case-control ratio of the target dataset. $P = 1.8 \times 10^{-4}$ for categorical NRI and $P = 2.4 \times 10^{-5}$ for continuous NRI. The p-values were calculated by the Z test for NRIs.

Consortia

The Tohoku Medical Megabank Project

Masayuki Yamamoto[2,10], Hikaru Abe[10], Michiaki Abe[10], Momoka Abe[10], Naomi Abe[10], Noriko Abe[10], Tomomi Abe[10], Tomomi Abe[10], Yuto Abe[10], Shizuko Ahiko[10], Kayo Aiki[10], Hiromi Aizawa[10], Yukari Akiyama[10], Hayato Anzawa[10], Eri Aoki[10], Yuichi Aoki[10], Hiroko Arai[10], Misaki Arakawa[10], Yukie Asano[10], Liam Baird[10], Ayano Chiba[10], Haruna Chiba[10], Ippei Chiba[10], Kenji Chiba[10], Keiko Chida[10], Inaho Danjoh[10], Hisako Endo[10], Reika Fue[10], Futaba Fujishiro[10], Yayoi Fujita[10], Waka Fukunaga[10], Takuo Fukushi[10], Mami Funata[10], Takamitsu Funayama[10], Sho Furuhashi[10], Nobuo Fuse[10], Kumiko Fushiya[10], Tomomi Gamo[10], Chinatsu Gocho[10], Katsuhiro Gonoi[10], Maki Goto[10], Takahiko Goto[10], Yukie Goto[10], Kaori Gouko[10], Michiko Haga[10], Yoko Haga[10], Yuko Hamada[10], Yohei Hamanaka[10], Mika Hanazawa[10], Yukari Hara[10], Hisano Hasebe[10], Atsushi Hasegawa[10], Hiroaki Hashizume[10], Asuka Hatakeyama[10], Sumika Hatakeyama[10], Nozomi Hatanaka[10], Rieko Hatanaka[10], Takanori Hidaka[10], Kenji Hino[10], Hiroe Hirama[10], Ikuo Hirano[10], Sachiko Hirano[10], Takumi Hirata[10], Masahiro Hiratsuka[10], Yuki Hiratsuka[10], Ikuko Hirayama[10], Eiji Hishinuma[10], Atsushi Hozawa[10], Keisuke Ido[10], Nobuko Igari[10], Chikako Iida[10], Katsuko Imai[10], Makiko Inoue[10], Marie Inoue[10], Reiko Inoue[10], Rumi Irie[10], Motoko Ishida[10], Noriko Ishida[10], Eri Ishigaka[10], Chihiro Ishii[10], Osamu Ishii[10], Tadashi Ishii[10], Tatsuro Ishikawa[10], Mami Ishikuro[10], Kazutoshi Ishimori[10], Ryosuke Ishiwata[10], Miho Itabashi[10], Maiko Ito[10], Masumi Ito[10], Mayumi Ito[10], Rie Ito[10], Saori Ito[10], Fumihiko Iwabuchi[10], Maki Iwabuchi[10], Yoko Izumi[10], Yoshiko Izumi[10], Masataka Kambe[10], Kanako Watanabe[10], Takanari Kanno[10], Mayu Kano[10], Naoko Kasahara[10], Hinako Kashiwa[10], Kiyomi Katahira[10], Mayumi Kato[10], Yukie Kato[10], Fumiki Katsuoka[10], Takeshi Kawabata[10], Rika Kawada[10], Aoi Kawagoe[10], Hiroshi Kawame[10], Junko Kawashima[10], Yukako Kawashima[10], Junko Kikuchi[10], Masahiro Kikuya[10], Masae Kimura[10], Kengo Kinoshita[10], Ikuko Kishi[10], Tomoko Kishimoto[10], Tamie Kitaura[10], Mika Kobayashi[10], Tadao Kobayashi[10], Tomoko Kobayashi[10], "Eiichi N." Kodama[10], Shun Kodate[10], Mana Kogure[10], Toshisada Kohagizawa[10], Naomi Kohketsu[10], Noa Koida[10], Chie Koide[10], Mika Koide[10], Toshihiko Koike[10], Shohei Koiso[10], Kaname Kojima[10], Junko Komatsu[10], Ayumi Kondo[10], Yukie Konno[10], Sachie Koreeda[10], Seizo Koshiba[10], Takuya Koyama[10], Hisaaki Kudo[10], Kazuki Kumada[10], Ryoko Kumadaki[10], Rika Kumagai[10], Toshie Kumagai[10],

Yuko Kumagai[10], Yasuto Kunii[10], Miho Kuriki[10], Shinichi Kuriyama[10], Miyuki Kuroda[10], Emiko Kurokawa[10], Seiko Kurota[10], Hisako Kusano[10], Bin Li[10], Donghan Li[10], Kanako Maeshibu[10], Keiko Maeta[10], Satoshi Makino[10], Hiroko Matsubara[10], Naomi Matsukawa[10], Masako Matsumoto[10], Takako Matsuoka[10], Yuka Matsushita[10], Fumiko Matsuzaki[10], Motomichi Matsuzaki[10], Hirohito Metoki[10], Sayaka Minakawa[10], Yuki Minami[10], Kyoko Mitate[10], Satomi Mito[10], Ayako Miura[10], Noriko Miura[10], Ryo Miyagi[10], Akiko Miyazawa[10], Satoshi Mizuno[10], Akiko Mochida[10], Mika Momii[10], Hiroko Mori[10], Naoko Mori[10], Hozumi Motohashi[10], "Ikuko N." Motoike[10], Shunji Mugikura[10], Keiko Murakami[10], Takahisa Murakami[10], Toshiro Muranishi[10], Masato Nagai[10], Satoshi Nagaie[10], Fuji Nagami[10], Tatsuo Nagasaka[10], Sachiko Nagase[10], Kumiko Nakagawa[10], Taku Nakai[10], Noriko Nakajo[10], Naoki Nakamura[10], Tomohiro Nakamura[10], Yuko Nakasato[10], Kumi Nakaya[10], Naoki Nakaya[10], Kei Nanatani[10], Natsuko Narisawa[10], Akira Narita[10], Yuka Narita[10], Hafumi Nishi[10], Kohji Nishida[10], Ichiko Nishijima[10], Takahiro Nobukuni[10], Kotaro Nochioka[10], Aoi Noda[10], Kenichi Noguchi[10], Kiriko Nozoe[10], Rie Nunokawa[10], Taku Obara[10], Tomoko Obara[10], Kaori Ogasawara[10], Satoru Ogawa[10], Soichi Ogishima[10], Nahoko Ohi[10], Namiko Ohisa[10], Kinuko Ohneda[10], Hayami Ohori[10], Yumi Oikawa[10], Yumiko Ojima[10], Yumi Okada[10], Yasunobu Okamura[10], Hiroshi Okuda[10], Mitsuko Okuda[10], Ayako Okumoto[10], Akane Ono[10], Chiaki Ono[10], Genki Onodera[10], Kaname Onodera[10], Masako Onodera[10], Midori Onuma[10], Tomomi Onuma[10], Keiichiro Oohashi[10], Masumi Oomachi[10], Kazuya Ootomo[10], Yukie Oouchi[10], Kazuko Oowada[10], Masatsugu Orui[10], Mayumi Osada[10], Tamae Osanai[10], Reiko Ota[10], Noriko Otake[10], Sumie Otomo[10], Tatsui Otsuka[10], Akihito Otsuki[10], Yoko Otsuki[10], Yuki Oyama[10], Keiko Oyamada[10], Masahiro Ozawa[10], Yoko Ozawa[10], Satomi Obara[10], Daisuke Saigusa[10], Asami Saito[10], Asuka Saito[10], Hisako Saito[10], Kazue Saito[10], Manami Saito[10], Megumi Saito[10], Ritsumi Saito[10], Sakae Saito[10], Tomo Saito[10], Yoshinobu Saitoh[10], Hiroko Sakai[10], Masaki Sakaida[10], Hiroshi Sakamono[10], Hiromi Sakamoto[10], Kana Sakamoto[10], Mia Sakamoto[10], Kasumi Sakurai[10], Miyuki Sakurai[10], Rieko Sakurai[10], Mika Sakurai-Yageta[10], Eriko Sasaki[10], Kana Sasaki[10], Miho Sasaki[10], Tadashi Sasaki[10], Yukari Sasaki[10], Yukie Sasaki[10], Akemi Sato[10], Chika Sato[10], Hirokazu Sato[10], Mayumi Sato[10], Michiyo Sato[10], Miho Sato[10], Mitsuharu Sato[10], Miu Sato[10], Naoko Sato[10], Reiko Sato[10], Satoshi Sato[10], Shiho Sato[10], Taku Sato[10], Yoshiko Sato[10], Youko Sato[10], Yui Sato[10], Yuriko Sato[10], Michihiro Satoh[10], Ayako Sekiya[10], Koji Shibuya[10], Hirohito

Shima[10], Yoshiko Shima[10], Muneaki Shimada[10], Ritsuko Shimizu[10], Genki Shinoda[10], Nobuyuki Shirakawa[10], Matsuyuki Shirota[10], Hiroe Shoji[10], Ikuko Shoji[10], Mariko Shoji[10], Midori Shoji[10], Wakako Shoji[10], Satomi Someya[10], Shinya Sonobe[10], Itsumi Sou[10], Rie Suenaga[10], Yasuko Suenaga[10], Mayumi Suga[10], Rika Sugai[10], Junichi Sugawara[10], Megumi Sugawara[10], Michiko Sugawara[10], Nanako Sugawara[10], Saori Sugawara[10], Yuki Sugawara[10], Sachiyo Sugimoto[10], Yoshiko Suto[10], Airi Suzuki[10], Ayano Suzuki[10], "Keiko P." Suzuki[10], Mariko Suzuki[10], Michirou Suzuki[10], Mikiko Suzuki[10], Norio Suzuki[10], Rie Suzuki[10], Ryoko Suzuki[10], Takafumi Suzuki[10], Tatsuya Suzuki[10], Yoichi Suzuki[10], Kaho Sato[10], Shu Tadaka[10], Keiko Taguchi[10], Nozomi Taiji[10], Makiko Taira[10], Kaori Takagi[10], Emi Takahashi[10], Harumi Takahashi[10], Junko Takahashi[10], Megumi Takahashi[10], Noriko Takahashi[10], Rieko Takahashi[10], Yukiko Takahashi[10], Mayuko Takasawa[10], Jun Takayama[10], Miho Takeuchi[10], Yoshinobu Takeyama[10], Sayaka Takita[10], Toru Tamahara[10], Gen Tamiya[2,4,10], Naomi Tamura[10], Akari Tanaka[10], Saiko Tanaka[10], Chihiro Tanno[10], Naoko Tanno[10], Keiko Tateno[10], Minoru Tateno[10], Chika Terui[10], Yuriko Tezuka[10], Mihoko Toki[10], Etsuko Tomita[10], Hiroaki Tomita[10], Mai Tomizuka[10], Akiko Toriyama[10], Naho Tsuchiya[10], Miyuki Tsuda[10], Tomomi Tsumuraya[10], Junko Tsunasawa[10], Issei Tsunoda[10], Juri Uchiya[10], Akiko Ueda[10], Yuriko Ueki[10], Fumihiko Ueno[10], Rumi Ujiie[10], Keiko Umeda[10], Akira Uruno[10], Ikuko Wada[10], Tomoko Wada[10], Mika Wagatsuma[10], Hitoshi Watanabe[10], Kazue Watanabe[10], Nobuo Yaegashi[10], Mika Yagyu[10], Etsuko Yamada[10], Yumi Yamaguchi-Kabata[10], Tomiko Yamauchi[10], Yukari Yamauchi[10], Mika Yamazaki[10], Kenji Yano[10], Jun Yasuda[10], Hang Yin[10], Hiroshi Yokota[10], Manami Yokoyama[10], Yuko Yoshida[10], Mizue Yoshino[10], Zhiqian Yu[10], Yoshiyuki Yukawa[10], Lin Zhang[10], Makoto Sasaki[14], Akimune Fukushima[14], Yasushi Ishigaki[14], Atsushi Shimizu[10,14], Koichi Asahi[14], Ryoichi Tanaka[14], Kozo Tanno[14], Kotaro Otsuka[14], Fumie Aizawa[14], Naoyuki Nishiya[14], Mitsuko Iwabuchi[14], Fumitaka Tanaka[14], Shinichi Omama[14], Kouhei Hashizume[14], Noriko Takebe[14], Kazuhiro Yoshikawa[14], Yuka Kotozaki[14], Masato Nagai[14], Takahiro Mikami[14], Takahito Nasu[14], Junko Akai[14], Yorihiro Koeda[14], Yohei Sawa[14], Nobuyuki Takanashi[14],Yayoi Yamasaki[14], Haruki Terui[14], Kasumi Hannokizawa[14], Hideki Ohmomo[14], Shohei Komaki[14], Mamoru Satoh[14], Yoichi Sutoh[14], Fumio Yamashita[14], Yutaka Hasegawa[14], Shiori Minabe[14], Tsuyoshi Hachiya[14], Tomoharu Tokutomi[14], Yukiko Toya[14], Akiko Yoshida[14], Satoshi Nishizuka[14] & Ryujin Endo[14]

The Biobank Japan Project

Koichi Matsuda[15,16], Yuji Yamanashi[17], Yoichi Furukawa[18], Takayuki Morisaki[19], Yukinori Okada[1,3,5,8,13], Yoshinori Murakami[20], Yoichiro Kamatani[11], Kaori Muto[21], Akiko Nagai[16], Yusuke Nakamura[22], Wataru Obara[23], Ken Yamaji[24], Kazuhisa Takahashi[25], Satoshi Asai[26,27], Yasuo Takahashi[27], Shinichi Higashiue[28], Shuzo Kobayashi[28], Hiroki Yamaguchi[29], Yasunobu Nagata[29], Satoshi Wakita[29], Chikako Nito[30], Yu-ki Iwasaki[31], Shigeo Murayama[32], Kozo Yoshimori[33], Yoshio Miki[34], Daisuke Obata[35], Masahiko Higashiyama[36], Akihide Masumoto[37], Yoshinobu Koga[37] & Yukihiro Koretsune[38]

14. Iwate Tohoku Medical Megabank Organization, Iwate Medical University, Iwate, Japan
15. Laboratory of Genome Technology, Human Genome Center, Institute of Medical Science, The University of Tokyo, Tokyo, Japan.
16. Laboratory of Clinical Genome Sequencing, Graduate School of Frontier Sciences, The University of Tokyo, Tokyo, Japan.
17. Division of Genetics, The Institute of Medical Science, The University of Tokyo, Tokyo, Japan.
18. Division of Clinical Genome Research, Institute of Medical Science, The University of Tokyo, Tokyo, Japan.
19. Department of Computational Biology and Medical Sciences, Graduate School of Frontier Sciences, BioBank Japan, Institute of Medical Science, The University of Tokyo, Tokyo, Japan.
20. Department of Cancer Biology, Institute of Medical Science, The University of Tokyo, Tokyo, Japan.
21. Department of Public Policy, Institute of Medical Science, The University of Tokyo, Tokyo, Japan.
22. The Institute of Medical Science, The University of Tokyo, Tokyo, Japan.
23. Department of Urology, Iwate Medical University, Iwate, Japan.

24. Department of Internal Medicine and Rheumatology, Juntendo University Graduate School of Medicine, Tokyo, Japan.

25. Department of Respiratory Medicine, Juntendo University Graduate School of Medicine, Tokyo, Japan.

26. Division of Pharmacology, Department of Biomedical Science, Nihon University School of Medicine, Tokyo, Japan.

27. Division of Genomic Epidemiology and Clinical Trials, Clinical Trials Research Center, Nihon University. School of Medicine, Tokyo, Japan.

28. Tokushukai Group, Tokyo, Japan.

29. Departmentof Hematology, Nippon Medical School, Tokyo, Japan.

30. Laboratory for Clinical Research, Collaborative Research Center, Nippon Medical School, Tokyo, Japan.

31. Department of Cardiovascular Medicine, Nippon Medical School, Tokyo, Japan.

32. Tokyo Metropolitan Geriatric Hospital and Institute of Gerontology, Tokyo, Japan.

33. Fukujuji Hospital, Japan Anti-Tuberculosis Association, Tokyo, Japan.

34. The Cancer Institute Hospital of the Japanese Foundation for Cancer Research, Tokyo, Japan.

35. Center for Clinical Research and Advanced Medicine, Shiga University of Medical Science, Shiga, Japan.

36. Department of General Thoracic Surgery, Osaka International Cancer Institute, Osaka, Japan.

37. Iizuka Hospital, Fukuoka, Japan.

38. National Hospital Organization Osaka National Hospital, Osaka, Japan.